Monolithic device for modelocking and stabilization of frequency combs

C.-C. Lee,[1*] Y. Hayashi,[2] K. L. Silverman,[3] A. Feldman,[3] T. Harvey,[3] R. P. Mirin,[3] and T. R. Schibli[1,4,5]

[1]*Department of Physics, University of Colorado at Boulder, 2000 Colorado Avenue, Boulder, CO 80309, USA*

[2]*Department of Electrical and Electronic Engineering, Tokyo Institute of Technology, Meguro-ku, Tokyo 152-8552, Japan*

[3]*National Institute of Standards and Technology, 325 Broadway, Boulder, CO 80305, USA*

[4]*JILA, National Institute of Standards and Technology and University of Colorado, Boulder, CO 80309, USA*

[5]*Department of Electrical, Computer and Energy Engineering, University of Colorado, Boulder, CO 80309, USA*

[*]*chienchung.lee@colorado.edu*

Abstract: We demonstrate a device that integrates a III-V semiconductor saturable absorber mirror with a graphene electro-optic modulator, which provides a monolithic solution to modelocking and noise suppression in a frequency comb. The device offers a pure loss modulation bandwidth exceeding 5 MHz and only requires a low voltage driver. This hybrid device provides not only compactness and simplicity in laser cavity design, but also small insertion loss, compared to the previous metallic-mirror-based modulators. We believe this work paves the way to portable and fieldable phase-coherent frequency combs.

OCIS codes: (320.7080) Ultrafast devices; (230.4110) Modulators; (230.0250) Optoelectronics; (230.5590) Quantum-well, -wire and -dot devices; (140.4050) Mode-locked lasers.

References and links

1. S. T. Cundiff and J. Ye, "Colloquium: Femtosecond optical frequency combs," Rev. Mod. Phys. **75**, 325–342 (2003).
2. S. A. Diddams, "The evolving optical frequency comb," J. Opt. Soc. Am. B **27**, B51–B62 (2010).
3. M. E. Fermann and I. Hartl, "Ultrafast fibre lasers," Nat. Photonics **7**, 868–874 (2013).
4. J. Lee, K. Lee, Y.-S. Jang, H. Jang, S. Han, S.-H. Lee, K.-I. Kang, C.-W. Lim, Y.-J. Kim, and S.-W. Kim, "Testing of a femtosecond pulse laser in outer space," Sci. Rep. **4**, 5134 (2014).
5. T. Wilken, M. Lezius, T. W. Hänsch, A. Kohfeldt, A. Wicht, V. Schkolnik, M. Krutzik, H. Duncker, O. Hellmig, P. Windpassinger, K. Sengstock, A. Peters, and R. Holzwarth, "A frequency comb and precision spectroscopy experiment in space," in *CLEO: 2013* (Optical Society of America, 2013), pp. AF2H.5.
6. L. C. Sinclair, I. Coddington, W. C. Swann, G. B. Rieker, A. Hati, K. Iwakuni, and N. R. Newbury, "Operation of an optically coherent frequency comb outside the metrology lab," Opt. Express **22**, 6996–7006 (2014).
7. U. Keller, "Ultrafast solid-state laser oscillators: a success story for the last 20 years with no end in sight," Appl. Phys. B **100**, 15–28 (2010).
8. T. M. Fortier, M. S. Kirchner, F. Quinlan, J. Taylor, J. C. Bergquist, T. Rosenband, N. Lemke, A. Ludlow, Y. Jiang, C. W. Oates, and S. A. Diddams, "Generation of ultrastable microwaves via optical frequency division," Nat. Photonics **5**, 425–429 (2011).
9. R. J. Jones, K. D. Moll, M. J. Thorpe, and J. Ye, "Phase-coherent frequency combs in the vacuum ultraviolet via high-harmonic generation inside a femtosecond enhancement cavity," Phys. Rev. Lett. **94**, 193201 (2005).
10. C. Benko, A. Ruehl, M. J. Martin, K. S. E. Eikema, M. E. Fermann, I. Hartl, and J. Ye, "Full phase stabilization of a Yb:fiber femtosecond frequency comb via high-bandwidth transducers," Opt. Lett. **37**, 2196–2198 (2012).

#248802 Received 10 Sep 2015; revised 16 Nov 2015; accepted 23 Nov 2015; published 15 Dec 2015

11. C.-C. Lee, C. Mohr, J. Bethge, S. Suzuki, M. E. Fermann, I. Hartl, and T. R. Schibli, "Frequency comb stabilization with bandwidth beyond the limit of gain lifetime by an intracavity graphene electro-optic modulator," Opt. Lett. **37**, 3084–3086 (2012).
12. M. Hoffmann, S. Schilt, and T. Südmeyer, "CEO stabilization of a femtosecond laser using a SESAM as fast opto-optical modulator," Opt. Express **21**, 30054–30064 (2013).
13. C.-C. Lee, S. Suzuki, W. Xie, and T. R. Schibli, "Broadband graphene electro-optic modulators with sub-wavelength thickness," Opt. Express **20**, 5264–5269 (2012).
14. N. Newbury and B. Washburn, "Theory of the frequency comb output from a femtosecond fiber laser," IEEE J. Quantum Electron. **41**, 1388–1402 (2005).
15. F. Wang, Y. Zhang, C. Tian, C. Girit, A. Zettl, M. Crommie, and Y. R. Shen, "Gate-variable optical transitions in graphene," Science **320**, 206–209 (2008).
16. Z. Q. Li, E. A. Henriksen, Z. Jiang, Z. Hao, M. C. Martin, P. Kim, H. L. Stormer, and D. N. Basov, "Dirac charge dynamics in graphene by infrared spectroscopy," Nat. Physics **4**, 532–535 (2008).
17. M. Liu, X. Yin, E. Ulin-Avila, B. Geng, T. Zentgraf, L. Ju, F. Wang, and X. Zhang, "A graphene-based broadband optical modulator," Nature **474**, 64–67 (2011).
18. N. Kuse, C.-C. Lee, J. Jiang, C. Mohr, T. R. Schibli, and M. Fermann, "Ultra-low noise all polarization-maintaining Er fiber-based optical frequency combs facilitated with a graphene modulator," Opt. Express **23**, 24342–24350 (2015).
19. C.-C. Lee and T. R. Schibli, "High-bandwidth, single-pole control of intracavity power in a mode-locked laser based on co-doped gain medium," in *CLEO: 2013* (Optical Society of America, 2013), pp. CTh1H.6.
20. M. Liu, X. Yin, and X. Zhang, "Double-layer graphene optical modulator," Nano Letters **12**, 1482–1485 (2012).
21. P. Rutter, K. Singer, and A. Peaker, "The incorporation of erbium into molecular beam epitaxy grown gallium arsenide," J. Cryst. Growth **182**, 247–254 (1997).
22. F. Ospald, D. Maryenko, K. von Klitzing, D. C. Driscoll, M. P. Hanson, H. Lu, A. C. Gossard, and J. H. Smet, "1.55μm ultrafast photoconductive switches based on ErAs:InGaAs," Appl. Phys. Lett. **92**, 131117 (2008).
23. X. Li, W. Cai, J. An, S. Kim, J. Nah, D. Yang, R. Piner, A. Velamakanni, I. Jung, E. Tutuc, S. K. Banerjee, L. Colombo, and R. S. Ruoff, "Large-area synthesis of high-quality and uniform graphene films on copper foils," Science **324**, 1312–1314 (2009).
24. I. Hartl, L. Dong, M. E. Fermann, T. R. Schibli, A. Onae, F. L. Hong, H. Inaba, K. Minoshima, and H. Matsumoto, "Fiber based frequency comb lasers and their applications," in *Advanced Solid-State Photonics* (Optical Society of America, 2005), pp. WE4.

1. Introduction

Modelocking-based frequency combs have been evolving rapidly in the last two decades from the classic Ti:sapphire bulk lasers to compact fiber-based lasers [1–3]. The driving force of this decade-long effort is indeed the desire to utilize frequency combs outside of an optics laboratory. Until recently, a number of such demonstrations have been reported [4–6], where fiber-based systems clearly dominate. Though fiber-based systems offer an advantage over free-space ones in terms of environmental sensitivity, it is crucial to have an all polarization-maintaining (PM) oscillator and carrier-envelope offset frequency (f_{ceo}) detection setup to avoid influences of temperature, stress, or vibration, which is an issue in non-PM systems. When one considers the available modelocking techniques that are feasible for turn-key, polarization-maintaining, and self-starting operation, the use of semiconductor saturable absorber mirrors (SESAMs) [7] is favored in many cases, although alternative techniques such as a nonlinear optical loop mirror can also be employed in an all polarization-maintaining way.

While the use of SESAM allows straightforward modelocking of a compact laser, two fast actuators are needed to suppress the noise in both the pulse repetition frequency (f_{rep}) and the carrier-envelope offset frequency (f_{ceo}). For metrological, long-term (>1s) applications, slow actuators are often sufficient. However, when short-term stability (1μs-1s) is of concern, high feedback bandwidth is required, for instance for the generation of ultralow-noise microwaves by direct frequency division [8], or for the generation of high-order harmonics with an enhancement cavity [9]. To stabilize f_{rep}, one can use a fast piezo or a lithium-niobate-based modulator that controls the cavity length, with up to ~1MHz bandwidth. For f_{ceo} stabilization, the conventional method of pump power modulation has fairly limited bandwidth due to the long stimulated gain lifetime in bulk lasers, especially rare-earth-doped ones.

#248802 Received 10 Sep 2015; revised 16 Nov 2015; accepted 23 Nov 2015; published 15 Dec 2015

A number of high-bandwidth approaches have been shown, including extra-cavity error correction with an acoustic-optic modulator (f_{3dB} ∼250kHz) [10], intracavity loss modulation with a graphene modulator (f_{3dB} ∼1MHz) [11], and opto-optical modulation with a SESAM (f_{3dB} ∼100kHz) [12]. Ideally one would like to have a device that can be introduced into the laser cavity without degrading the modelocking performance and without complicating the cavity design. In our first demonstration of graphene modulators and its use in a laser cavity [11, 13], one had to slightly modify the laser cavity to accommodate the graphene modulator as an end mirror, which was an added complication and may not be compatible with certain type of lasers. A monolithic solution is therefore desirable, especially for fieldable frequency combs with an all-fiber linear cavity [6].

We demonstrate in this work a new generation of graphene electro-optic modulators that are integrated with a SESAM. This monolithic device provides electro-optic loss modulation from graphene as well as saturable loss from an InGaAs quantum well. The optical loss of graphene can be modulated with a low-voltage electrical signal, and the introduced cavity loss modulation offers an unconventional advantage over the pump power modulation technique since loss modulation bypasses the gain medium and therefore offers a modulation bandwidth beyond the limit of the gain lifetime [11, 14]. We envision the use of this novel device in compact, fieldable frequency combs where ultralow integrated phase noise level ($<$100 mrads) is required, such as a portable low-noise microwave generator.

2. Design considerations and device fabrication

The first demonstration of graphene modulators suitable for intracavity loss modulation [13] utilized a metallic thin film (silver) as a highly-reflective optical mirror and as an electrode, which enabled modulation of Fermi level (thus optical absorption) in graphene [15–17]. Despite its simple structure and applicability in fiber-based lasers [11, 18], the use of a metal-based mirror led to some optical loss that may not be tolerable in solid-state bulk lasers. The optical loss can be reduced by using a dielectric Bragg reflector with a very thin (few nanometers) metallic layer located at the node of the optical fields, which serves as a transparent electrode [19], although the effective optical bandwidth of the Bragg reflector is reduced due to the presence of the metallic film. A suitable low-optical-loss transparent electrode is desirable without the trade-off between optical loss and optical bandwidth of the mirror. It should be noted that graphene itself is a good transparent, electrically conducting material. This enables one to fabricate an optical modulator with graphene on both sides of the gate dielectric [20], provided that high-quality dielectric, such as aluminum oxide realized by atomic layer deposition, can be deposited on graphene without compromising its crystalline quality. In this work, the transparent electrode issue is naturally resolved because we can utilize the electronic and optical properties of gallium arsenide (GaAs) that a shallowed-doped layer provides sufficient electrical conductivity while its linear optical absorption remains small. The SESAM therefore can serve not only as a saturable absorber for modelocking but also as a transparent electrode for gating the graphene modulator. This allows the realization of a low-loss device suitable for even the most optical-loss-aversive bulk lasers.

A schematic drawing of the device is shown in Fig. 1(a), and a scanning electron microscope image of the SESAM, before modulator fabrication, is shown in Fig. 1(b). The calculated optical fields in the device are shown in Fig. 1(c), with and without the dielectric in the modulator. The device consists of a Bragg reflector(24 pairs of GaAs/AlAs), a 10-nm-thick InGaAs:Er quantum well(QW), a cap 110-nm GaAs layer, and a graphene modulator. The SESAM, grown by molecular beam epitaxy, was designed for modelocking at the center wavelength of 1560 nm, and ultrafast recombination centers were introduced in the absorber by a low temperature (LT) growth at 475°C. We used erbium doping in the InGaAs QW to ensure an ultrafast re-

#248802 Received 10 Sep 2015; revised 16 Nov 2015; accepted 23 Nov 2015; published 15 Dec 2015

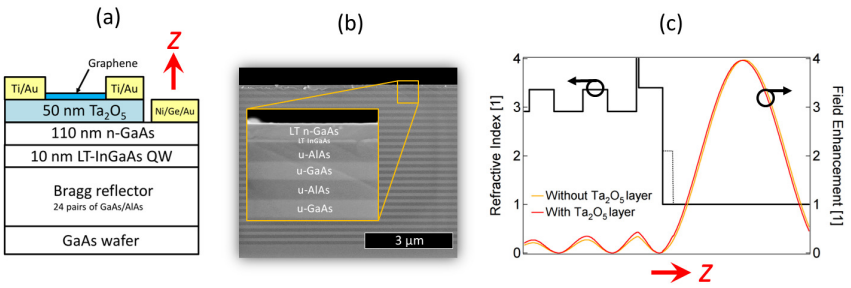

Fig. 1. (a) Cross-sectional view of the hybrid graphene-SESAM device. (b) Scanning electron microscope image of the SESAM structure, which has been cleaved for inspection. (c) Plot of refractive index and electric field (optical) enhancement as a function of position in the z direction, as specified with a red arrow. The field enhancement is defined as the ratio of the square modulus of local fields to that of the incident wave and is calculated based on a transfer-matrix approach. The addition of a 50-nm Ta_2O_5 layer only slightly affects the field distribution in the device.

sponse time of the SESAM. At doping levels used during this growth (5×10^{18} cm^{-3}), ErAs precipitates have been shown to form in GaAs which efficiently trap photo-excited carriers [21]. A similar situation is expected to occur in InGaAs:Er QWs and, in fact, ErAs has been included in bulk InGaAs to facilitate ultrafast photoconductive switches [22]. Silicon was introduced as n-dopant in the top GaAs layer with a concentration of $\sim 5 \times 10^{17}$ cm^{-3}, which results in a sheet resistance of ~ 800 k$\Omega/\square$. The poor electrical conductivity likely arose from the LT-induced lattice defects. An annealing step (rapid thermal annealing at 500°C for 30 seconds) was introduced before the modulator fabrication to reduce the sheet resistance.

This doped layer serves as a transparent electrode for the graphene modulator. The modulator is comprised of a 50-nm tantalum oxide(Ta_2O_5) layer as the gate dielectric, wet-transferred chemical-vapor-deposition(CVD)-grown graphene [23], and top and bottom metal contacts, as shown in Fig. 1. It is crucial to use Ni/Ge/Au as the contact material on n-GaAs in order to achieve low contact resistance and ohmic behavior. In our device, 20 nm of Ni and 80 nm of Ge/Au eutectic alloy were thermally evaporated onto the SESAM. The sample was then annealed in a rapid thermal annealing (RTA) furnace for 120 seconds at 350°C in order to form ohmic contact. The 50-nm Ta_2O_5 was deposited using DC reactive sputtering. The top contact, which consists of 10 nm of Ti and 90 nm of Au, was also thermally evaporated. After that, CVD-graphene was transferred directly on the top contact. Oxygen plasma etch was then performed on graphene to make suitable active apertures and remove parasitic capacitance.

Because the capacitance of the graphene/Ta_2O_5/n-GaAs structure couples with the sheet resistance of the n-GaAs layer, the modulation bandwidth of the graphene modulator is determined by an equivalent RC circuit. Since the capacitance scales linearly with area, it is crucial to keep the sheet resistance of n-GaAs layer low, which we have achieved using shallow silicon doping and annealing. For this demonstration, we show a modulator with an active aperture of 200 μm in diameter, which is large enough for most intracavity applications.

3. Device characterization results

Various annealing conditions for improving the conductivity of the n-GaAs layer have been investigated. The changes in sheet resistance and the absorption-induced-carrier recovery time is shown in Fig. 2, where the recovery time of the annealed SESAM showed an increased amount of slow recovery compared to the condition before annealing. The measurement was

#248802 Received 10 Sep 2015; revised 16 Nov 2015; accepted 23 Nov 2015; published 15 Dec 2015

performed with a 1560 nm wavelength, 125 fs pulse width, 88 MHz repetition-rate modelocked laser on SESAMs without graphene. It was found that annealing at 500°C resulted in a low sheet resistance of $\sim$ 16 k$\Omega/\square$ and that beyond 600°C, the sheet resistance increased slightly, and the fast component of relaxation almost vanished. In Fig. 2(c), the corresponding plot of optical reflectivity of the SESAM before annealing is shown. No measurable change in the saturable absorption curve was observed after annealing except non-saturable loss. However sample-to-sample variation and measurement uncertainty ($\pm$0.5%) have prevented us from drawing a conclusion about the annealing-induced-change in non-saturable loss due to the small value of the total loss. The group delay dispersion of the SESAM is about -100fs^2 at 1550 nm, and no optical damage was observed in the nonlinear absorption measurement, with a maximum pulse fluence of $\sim 3\ \text{mJ}/\text{cm}^2$.

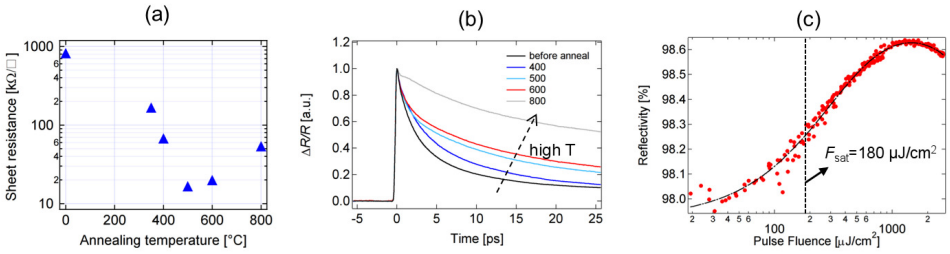

Fig. 2. Physical properties of SESAM, without graphene. (a) Sheet resistance versus annealing temperature. Before annealing is denoted by 0°C. (b) Carrier relaxation dynamics in sample before and after annealing. With a bi-exponential fit function $\Delta R/R = A_1 e^{-t/\tau_1} + A_2 e^{-t/\tau_2}$, the recovery times ($\tau_1$, τ_2) and the ratio of fast to slow relaxation (A_1/A_2) are found to be τ_1 $\sim$2 ps, τ_2 $\sim$21 ps, and $A_1/A_2 = 1.9$ in the un-annealed sample; τ_1 $\sim$1 ps, τ_2 $\sim$16 ps, and $A_1/A_2 = 0.5$ in the 500°C-annealed sample. (c) Nonlinear absorption characterization of the absorber, before annealing. Using a slow-absorber fit function with two-photon absorption, $\Delta R = q_0(F_{\text{sat}}/F)(1 - e^{-F/F_{\text{sat}}}) - \beta_{\text{TPA}}\ell_{\text{TPA}}(F/\tau_{\text{pulse}})$, we found $q_0 \sim$ 0.9%(saturable loss), $F_{\text{sat}} \sim 180\ \mu\text{J}/\text{cm}^2$(pulse fluence), $\beta_{\text{TPA}}\ell_{\text{TPA}} \sim 10^3\text{cm}\cdot\text{nm}/\text{GW}$(two-photon-absorption coefficient$\times$layer thickness), and a non-saturable loss $\sim$ 1.1%.

The thickness of the high-k dielectric can be chosen to tailor the insertion loss from graphene and the corresponding modulation depth. In this particular device, an average modulation depth of $\sim$ 0.07%(pk-pk) at 100kHz was observed across an active aperture of 200 μm with only 5.6 V_{pp} applied to the device (Fig. 3), which was measured by raster scanning a tightly focused low-power continuous-wave laser centered at 1550 nm while recording the percentage of modulation in the reflected optical power. An optical reflectivity map is also shown in Fig. 3(b), an average reflectivity of 98.5$\pm$0.5% was found. We presume the slight increase in reflectivity was due to the reduction of defect-induced non-saturable loss after thermal annealing at 500°C.

The frequency response of the graphene modulator was measured with a network analyzer, as shown in Fig. 4(a). The 3-dB bandwidth was found to be $\sim$5.6 MHz, measured relative to the peak. This bandwidth is sufficient for most f_{ceo} noise or relative intensity noise (RIN) suppression in lasers. The modulation depth as a function of applied modulation signal amplitude (Fig. 4(b)) shows good linearity up to 14 V_{pp}, which corresponds to $\sim$ 1.4 MV/cm field strength in the Ta_2O_5 layer. The maximum modulation depth is limited by the electrical breakdown in Ta_2O_5.

At low frequencies (1 kHz to 100 kHz), it can be seen that the response of the modulator is reduced, which we hypothesize to be caused by the presence of free charges in the GaAs layer screening the applied field. These carriers may be generated from charge traps or across the bandgap and can only follow the field below 100 kHz. Since the intended use of the graphene

#248802 Received 10 Sep 2015; revised 16 Nov 2015; accepted 23 Nov 2015; published 15 Dec 2015

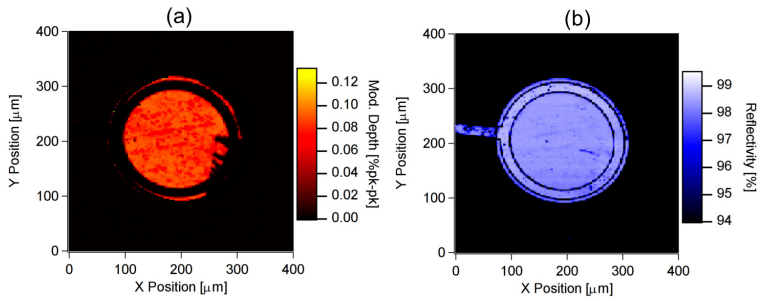

Fig. 3. (a) Heatmap of the modulation depth of the graphene modulator. (b) Heatmap of the optical reflectivity of the device, taken simultaneously with the modulation depth.

modulator is a fast actuator for noise suppression and is usually paired with a slow counterpart, such as pump power modulation or temperature control of a fiber-based Bragg grating [24], the reduced low-frequency response should not be of a big concern. Nevertheless, the suppressed low-frequency response might be improved in the future by, for example, proper DC biasing of the device or reduction of the charge traps in GaAs.

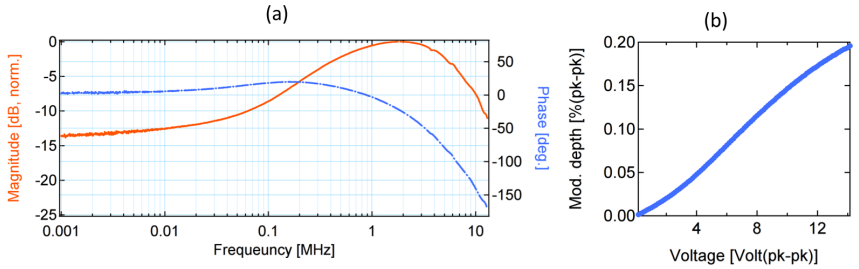

Fig. 4. (a) Transfer function of the graphene modulator. The voltage applied is $2V_{pp}$. (b) Modulation depth measured as a function of applied ac voltage amplitude at 100 kHz.

4. Conclusion

We have demonstrated a dual-function device that serves as a saturable absorber for mode-locking and as a cavity loss modulator with a modulation bandwidth beyond 5MHz. The total insertion loss of the device was measured to be $\sim 1.5\%$, and graphene modulator showed a modulation depth of 0.2% with 14 V_{pp} applied. Even though this demonstration is targeting at lasers at 1.5 μm wavelength, the fabrication techniques and design principles should be applicable to other wavelengths of interest. This hybrid device is believed to help boost the noise suppression bandwidth in compact frequency combs that are finding applications where excellent short-time stability is needed.

Acknowledgments

We thank Dr. Tomoko Borsa for her help with the SEM. This work was supported by the DARPA PULSE program with a grant from AMRDEC(W31P4Q-14-1-0001), by the NSF Early Career Award(1253044), and by the NSF under Grant No. ECCS-0335765.